ChemComm

RSC Publishing

COMMUNICATION

View Article Online
View Journal | View Issue



# Spectroscopic properties and reactivity of a mononuclear oxomanganese(IV) complex†

Cite this: *Chem. Commun.*, 2013, **49**, 5378

Received 10th January 2013,
Accepted 25th April 2013

DOI: 10.1039/c3cc00244f

www.rsc.org/chemcomm

Domenick F. Leto, Rena Ingram, Victor W. Day and Timothy A. Jackson*

**A non-porphyrinic, mononuclear oxomanganese(IV) complex was generated at room temperature and characterized by spectroscopic methods. The $Mn^{IV}$=O adduct is capable of activating C–H bonds by a H-atom transfer mechanism and is more reactive in this regard than most $Mn^{IV}$=O species.**

High-valent oxomanganese adducts are suggested as active oxidants for synthetic and biological manganese catalysts, including those involved in textile and paper bleaching with $H_2O_2$ and oxygen evolution from water.[1] Oxomanganese(V) adducts with $S$ = 0 and 1 spin states have been reported, and these invariably feature strongly electron-donating, anionic ligands.[2] Oxomanganese(IV) complexes with neutral, non-porphyrinic ligands are comparatively less common.[3] Detailed studies of substrate oxidation exist for a limited number of complexes.[3a–c,4] In addition, few $Mn^{IV}$=O complexes have been characterized by Mn K-edge X-ray absorption spectroscopy (XAS),[3b,5] a technique featuring prominently in the study of Mn enzymes[1b] and biominerals.[6] In this report, we describe the spectroscopic properties and oxidative reactivity of an oxomanganese(IV) complex supported by the neutral, pentadentate N4py ligand (*N*,*N*-bis(2-pyridylmethyl)-*N*-bis(2-pyridyl)methylamine). This $Mn^{IV}$=O compound is more reactive than the majority of $Mn^{IV}$=O complexes for C–H bond oxidation.

The manganese(II) complex $[Mn^{II}(N4py)]^{2+}$ (**1**) was generated as the triflate salt. The X-ray diffraction (XRD) structure exhibits a distorted octahedral $Mn^{II}$ center with pentadentate N4py and monodentate triflate ligands (Fig. 1A). The Mn–ligand bond lengths are 2.1 to 2.3 Å. The Mn K-edge XAS spectrum of a frozen aqueous sample of **1**$(OTf)_2$ displays a pre-edge feature at 6540.6 eV and an edge at 6547.3 eV. The EXAFS data are best fit with 1 O at 2.09 Å, 5 N at 2.26 Å, and 3 C at 3.00 Å, in excellent agreement with the XRD structure (*cf.* Tables S4 and S6; ESI†).

The addition of excess PhIO (2.5 equiv.) to **1** in $CF_3CH_2OH$ at 298 K led to the formation of a green species (**2**), with a broad

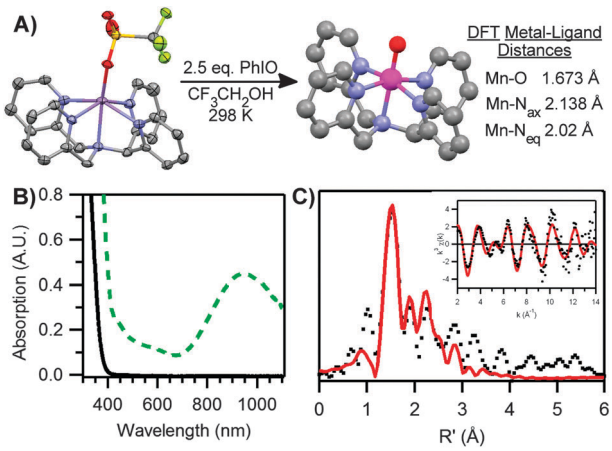


**Fig. 1** (A) XRD structure of $[Mn^{II}(N4py)(OTf)]^+$ (**1**(OTf), left) and DFT (BP/TZVP) structure of $[Mn^{IV}(O)(N4py)]^{2+}$ (**2**, right). Hydrogen atoms are omitted for clarity. (B) 298 K electronic absorption spectra of **1** (black solid trace) and **2** (green dashed trace); both 2 mM in $CF_3CH_2OH$. (C) Fourier transform of the Mn K-edge EXAFS data and EXAFS spectrum (inset), experimental data (···) and fits (–), for **2** in $CF_3CH_2OH$.

electronic absorption band at 950 nm and weaker features at 600 and 450 nm (Fig. 1B). At 298 K, the formation of **2** finished in ~10 minutes, and **2** showed a half-life of 30 minutes. The absorption features of **2** are very similar to those of other non-porphyrinic $Mn^{IV}$=O complexes in tetragonal, six-coordinate environments, which display broad near-infrared bands from ~1040–825 nm and weaker features at higher energies.[3a,b,7] The perpendicular mode X-band EPR spectrum of **2** is typical of a mononuclear, $S$ = 3/2 $Mn^{IV}$ ion (Fig. S4; ESI†).[3a,b,d,8] Hyperfine coupling for the $g_{eff}$ = 5.76 feature is ~76 G, in good agreement with that observed for other $Mn^{IV}$=O complexes.[3d] High-resolution electrospray-ionization mass spectral (ESI-MS) data of **2** reveal a major ion peak at $m/z$ 219.0502, consistent with $[Mn^{IV}(O)(N4py)]^{2+}$ ($m/z$ calc. 219.0563). When **2** is spiked with 10 μL $H_2{}^{18}O$ (97% $^{18}O$-enriched), a new molecular ion peak is observed at $m/z$ 220.0537, indicating incorporation of $^{18}O$ from $H_2{}^{18}O$ ($[Mn^{IV}(^{18}O)(N4py)]^{2+}$ $m/z$ calc. 220.0585). These data together support the formulation of **2** as $[Mn^{IV}(O)(N4py)]^{2+}$.

As we have been unable to grow crystals of **2**, its molecular structure was investigated by Mn K-edge XAS. The edge energy

*Department of Chemistry, The University of Kansas, 1251 Wescoe Hall Drive, Lawrence, KS, USA. E-mail: taj@ku.edu; Fax: +1-785-864-5396; Tel: +1-785-864-3968*

† Electronic supplementary information (ESI) available: Details of experimental and kinetic procedures. CCDC 885972. For crystallographic data in CIF or other electronic format see DOI: 10.1039/c3cc00244f

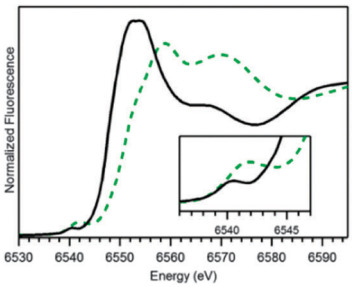


**Fig. 2** 20 K Mn K-edge XAS near-edge region of **1**$(OTf)_2$ (black solid trace) and **2** (green dashed trace) in $H_2O$ and $CF_3CH_2OH$, respectively.

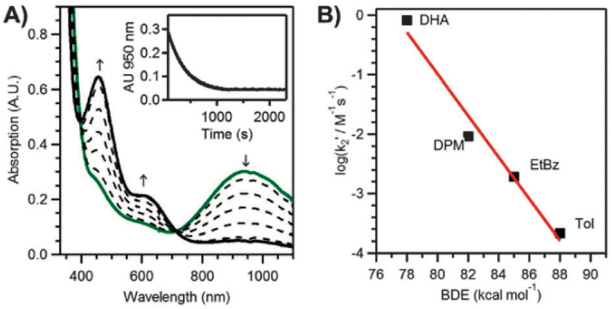


**Fig. 3** (A) Electronic absorption spectra of **2** upon addition of 200 equiv. EtBz in $CF_3CH_2OH$ at 298 K. Inset: decay of the 950 nm absorption signal. (B) Corrected second-order rate constant ($k_2'$) *versus* bond dissociation enthalpies of organic substrates.

of **2** (6550.8 eV) is blue-shifted over 3 eV relative to that of **1**, as expected for the higher oxidation state of Mn (Fig. 2). The edge energy of **2** is within 1 eV of those reported for $Mn^{IV}$═O complexes supported by salen and porphyrin ligands (6549.9–6551.2 eV; Table S3; ESI†).[5] The pre-edge peak of **2** at 6541.9 eV is significantly more intense than that of **1** (Fig. 2, inset), consistent with a large deviation from centrosymmetry.

The Fourier transform ($R'$ space) of the EXAFS data of **2** exhibits a prominent, sharp peak at $R' \approx 1.5$ Å with less prominent peaks at $R' \approx 1.9$, 2.2, and 2.8 Å (Fig. 1C). The first coordination sphere of **2** is fit well with two or three shells of N/O atoms at distances ($r$) of 1.69, 2.00, and 2.24 Å (Table S4; ESI†). The shell at 1.69 Å, which corresponds to the oxo ligand, is much shorter than the $Mn^{II}$–O (solvent $H_2O$) distance of 2.09 Å observed for **1**. The remaining first coordination sphere can be fit with either a single shell of 5 nitrogen scatterers at 1.99 Å or two shells of nitrogen scatterers at 2.00 Å (4 N atoms) and 2.24 Å (1 N atom), representing the nitrogen atoms of the pentadentate N4py ligand. The fit with two shells of N scatterers affords lower GOF and Debye–Waller values than the fit with just one shell of five N scatterers. Fits including outer-sphere features reveal two Mn···C shells at 2.82 and 2.97 Å (3 and 5 C atoms, respectively).

Metric parameters from the EXAFS data of **2** are in good agreement with a DFT-computed structure (Fig. 1A, right). This structure has a Mn═O bond of 1.673 Å (*cf.* the EXAFS distance of 1.69 Å). The equatorial nitrogens in the DFT-optimized structure have an average Mn–N distance of 2.024 Å, while the *trans* amine has a longer distance of 2.138 Å, consistent with the two shells of Mn–N scatterers at 2.00 and 2.24 Å.

The ability of **2** to activate C–H bonds was investigated using dihydroanthracene (DHA), diphenylmethane (DPM), ethylbenzene (EtBz), and toluene (Tol), which span a ~10 kcal $mol^{-1}$ range of C–H bond strengths. For each substrate, the addition of an excess to **2** at 298 K under an Ar atmosphere led to (i) a disappearance in the optical bands of **2**, (ii) formation of a new species, **3**, with bands at 460 and 630 nm, and (iii) the appearance of an isosbestic point at 714 nm (Fig. 3A). The decay of **2** and the formation of **3** occurred with the same rate, both following pseudo-first order behaviour to at least four half-lives (see ESI†). Second-order rate constants ($k_2'$, corrected for the number of reactive C–H bonds) determined for all substrates revealed a linear relationship between $\log(k_2')$ and substrate bond dissociation enthalpies (BDEs), with a slope of 0.35 (Fig. 3B). Such behaviour is highly suggestive of a rate-limiting H-atom transfer.[3a] In support, reactions of **2** with deuterated-DHA ($d_4$-DHA) reveal a kinetic isotope effect (KIE) of 11.2, which is larger than that observed for DHA oxidation by other $Mn^{IV}$═O adducts (3.1–8).[2c,3a,4a,9] Activation energies ($E$) and Arrhenius prefactors ($A$) determined from the reaction of **2** with DHA and $d_4$-DHA from 35 to −5 °C in 1 : 1 $CF_3CH_2OH$ : $CH_2Cl_2$ provide evidence for H-atom tunnelling (Table S10; ESI†). Specifically, the difference in activation energies for DHA and $d_4$-DHA ($E_D - E_H$) is greater than the difference in zero-point energies of the C–H and C–D bonds (3.6 and 1.26 kcal $mol^{-1}$, respectively); and the ratio of Arrhenius prefactors ($A_H/A_D$ = 0.02) is much less than 0.7, and comparable to that of $[Fe^{IV}(O)(N4py)]^{2+}$, where a H-atom tunnelling mechanism was also implicated.[10] The reaction of **2** with DHA proceeded with a second-order rate constant ($k_2'$ = 3.6 $M^{-1}$ $s^{-1}$) 2–3 orders of magnitude larger than those observed at similar temperatures for nearly all other non-porphyrinic $Mn^{IV}$═O complexes (Table S8; ESI†).[3a,4a,9,11] An Eyring analysis of DHA activation from 35 to −5 °C, reveal $\Delta H^{\ddagger}$ and $\Delta S^{\ddagger}$ of 9 ± 0.8 kcal $mol^{-1}$ and −35 ± 3 cal $mol^{-1}$ K, respectively (Table S9; ESI†). These parameters yield a $\Delta G^{\ddagger}$ (at 25 °C) comparable to that of $[Mn^{IV}(O)(H_3buea)]^-$ but 2 kcal $mol^{-1}$ smaller than those observed for other $Mn^{IV}$═O complexes,[3a,4a,b] consistent with the greater reactivity of **2**.

The reaction of **2** with DHA yielded 0.56(8) equiv. of anthracene per equiv. of **2**. A final Mn oxidation state of 2.7(15) was determined by iodometric titration. This product distribution is consistent with the generation of anthracene by reaction of 1 equiv. DHA with 2 equiv. $Mn^{IV}$═O rather than two successive H-atom transfers with a single $Mn^{IV}$═O centre. Thus, **2** acts as a one-electron oxidant, which has been observed for other $Mn^{IV}$═O compounds.[2c,3a,b,4c] Such reactivity is consistent with DFT studies by Shaik and Nam that have shown a second H-atom transfer between the nascent organic radical and $Mn^{III}$–OH centre to be less favorable than diffusion of the organic radical from the $Mn^{III}$–OH adduct.[12] To the best of our knowledge, two-electron oxidation of DHA by a $Mn^{IV}$═O has only been observed for $[Mn^{IV}(O)_2(Me_2EBC)]^+$ and $[Mn^{IV}(O)(OH_2)(BQCN)]^{2+}$.[3c,4c]

While the iodometric product analysis gives an average Mn oxidation state following the reaction of **2** with DHA, the nature of the Mn-based products can be better defined on the basis of EPR, electronic absorption, and ESI-MS data. Perpendicular-mode EPR spectra of the product solution showed the strong $Mn^{IV}$═O signals replaced by very weak signals. Broad features over a large field range and a sharp multiline signal at $g \approx 2$ are respectively attributed to mononuclear $Mn^{II}$ and binuclear species (Fig. S5; ESI†). Corresponding parallel-mode EPR spectra are silent. This does not preclude the presence of mononuclear $Mn^{III}$ species,

as favourable $Mn^{III}$ zero-field splitting parameters and high-quality glasses are often required to observe the weak six-line signals of mononuclear $Mn^{III}$ centres in X-band experiments. The optical absorption features of product **3** are quite similar to those of $[Mn^{III}(OCH_2CF_3)(Bn\text{-}TPEN)]^{2+}$ (Bn-TPEN = *N*-benzyl-*N*,*N*′,*N*′-tris-(2-pyridylmethyl)-1,2-diaminoethane), which was the dominant Mn product when $[Mn^{IV}(O)(Bn\text{-}TPEN)]^{2+}$ was reacted with hydrocarbons.[3b] In addition, the dominant molecular ion peak in ESI-MS data of **3** is at *m*/*z* 620.1289, consistent with $[Mn^{III}(OCH_2CF_3)(N4py)](OCH_2CF_3)^+$ (*m*/*z* calc. 620.1293). Thus, we propose a mononuclear $Mn^{III}$ species as the dominant, but not sole, Mn-based product when **2** reacts with DHA.[13]

The chemical reactivity of **2** is similar to that of $[Mn^{IV}(O)(Bn\text{-}TPEN)]^{2+}$.[3b] Both N4py and Bn-TPEN are N5 aminopyridyl ligands that also support highly reactive $Fe^{IV}$═O complexes.[10] For the $Mn^{IV}$═O adducts, previous DFT computations predicted that **2** has a larger barrier for H-atom abstraction from cyclohexane than $[Mn^{IV}(O)(Bn\text{-}TPEN)]^{2+}$.[12] Although the addition of a large excess (400–600 equiv.) of cyclohexane increases the decay rate of **2**, the reaction does not show pseudo-first order behaviour. In contrast, $[Mn^{IV}(O)(Bn\text{-}TPEN)]^{2+}$ reacts with cyclohexane at 25 °C. Thus, we are unable to determine a $k_2$ value to provide a quantitative comparison of reactivity using cyclohexane. However, a comparison can be made using EtBz, with which both compounds react at 25 °C in $CF_3CH_2OH$. In the reaction with EtBz, $[Mn^{IV}(O)(Bn\text{-}TPEN)]^{2+}$ (1 mM) shows a rate constant five-fold larger than that of **2** (2 mM): $k_2' = 2.7 \times 10^{-2}$ and $5.7 \times 10^{-3}$ $M^{-1}$ $s^{-1}$, respectively. Thus, while **2** is dramatically more reactive towards C–H bonds than most $Mn^{IV}$═O adducts, it is less reactive than $[Mn^{IV}(O)(Bn\text{-}TPEN)]^{2+}$. This trend holds for the corresponding $Fe^{IV}$═O adducts; *i.e.*, $[Fe^{IV}(O)(Bn\text{-}TPEN)]^{2+}$ is more reactive towards C–H bonds.[10]

The origin of the high reactivity of **2** towards C–H bonds is currently unclear. Cyclic voltammetry studies of **2** show a $Mn^{III/IV}$ reduction potential ($E_{1/2}$) ~700 mV higher than those of other $Mn^{IV}$═O complexes (ESI†).[3a,4a,9] Thus, **2** is a significantly more effective one-electron oxidant. Notably the $E_{1/2}$ of **2** is similar to those of other dicationic $Mn^{IV}$ complexes,[3a,9] suggesting that the increase in $E_{1/2}$ is attributed to the +2 total charge of **2** *versus* the +1 and −1 charges of other $Mn^{IV}$═O adducts.[3a,4a] However, rates of H-atom transfer reactions, which are strongly correlated to thermodynamic driving force, depend not only on the reduction potential of the oxidant, but also on the basicity of the metal–hydroxo product.[14] Both the $Mn^{III/IV}$ reduction potential and the $pK_a$ of the $Mn^{III}$–OH complex, which for this system is unknown, are necessary for a thermodynamic analysis. While we cannot comment at present on the driving force for C–H bond activation by **2**, we note that many other $Mn^{IV}$═O adducts have sterically demanding supporting ligands that shield the oxo. In contrast, the oxo ligand in **2** is well-exposed to substrate (Fig. 1A). Reduced steric clash with substrate could contribute to the relatively high reactivity of **2**. Future work is needed to determine the role ligand sterics, solvent effects, and thermodynamic driving force play in influencing the H-atom transfer reactivity of **2**, and to explore further why $Mn^{IV}$═O adducts such as **2** may eschew standard rebound or desaturation mechanisms for C–H activation.

This work was supported by the US NSF (CHE-1056470 to T.A.J.; CHE-1004897 for R.I.; CHE-0946883 and CHE-0079282 supported instrument purchases). XAS experiments were supported by the Center for Synchrotron Biosciences grant, P30-EB-009998, from the National Institute of Biomedical Imaging and Bioengineering (NIBIB). We thank Dr Erik Farquhar at NSLS for outstanding support of our XAS experiments.

Most recently Chen *et al*. reported the formation and characterization of **2** and described the effects of $Sc^{3+}$ on oxo and H-atom transfer reactions.[12b]

## Notes and references

1 (*a*) J. P. McEvoy and G. W. Brudvig, *Chem. Rev.*, 2006, **106**, 4455–4483; (*b*) A. J. Wu, J. E. Penner-Hahn and V. L. Pecoraro, *Chem. Rev.*, 2004, **104**, 903–938; (*c*) R. Hage and A. Lienke, *Angew. Chem., Int. Ed.*, 2006, **45**, 206–222.
2 (*a*) D. E. Lansky, A. A. Narducci Sarjeant and D. P. Goldberg, *Angew. Chem., Int. Ed.*, 2006, **45**, 8214–8217; (*b*) K. A. Prokop, S. P. de Visser and D. P. Goldberg, *Angew. Chem., Int. Ed.*, 2010, **49**, 5091–5095; (*c*) C. Arunkumar, Y.-M. Lee, J. Y. Lee, S. Fukuzumi and W. Nam, *Chem.–Eur. J.*, 2009, **15**, 11482–11489; (*d*) J. T. Groves, J. Lee and S. S. Marla, *J. Am. Chem. Soc.*, 1997, **119**, 6269–6273; (*e*) T. Taguchi, R. Gupta, B. Lassalle-Kaiser, D. W. Boyce, V. K. Yachandra, W. B. Tolman, J. Yano, M. P. Hendrich and A. S. Borovik, *J. Am. Chem. Soc.*, 2012, **134**, 1996–1999; (*f*) T. J. Collins and S. W. Gordon-Wylie, *J. Am. Chem. Soc.*, 1989, **111**, 4511–4513.
3 (*a*) I. Garcia-Bosch, A. Company, C. W. Cady, S. Styring, W. R. Browne, X. Ribas and M. Costas, *Angew. Chem., Int. Ed.*, 2011, **50**, 5648–5653; (*b*) X. Wu, M. S. Seo, K. M. Davis, Y.-M. Lee, J. Chen, K.-B. Cho, Y. N. Pushkar and W. Nam, *J. Am. Chem. Soc.*, 2011, **133**, 20088–20091; (*c*) S. C. Sawant, X. Wu, J. Cho, K.-B. Cho, S. H. Kim, M. S. Seo, Y.-M. Lee, M. Kubo, T. Ogura, S. Shaik and W. Nam, *Angew. Chem., Int. Ed.*, 2010, **49**, 8190–8194; (*d*) T. H. Parsell, R. K. Behan, M. T. Green, M. P. Hendrich and A. S. Borovik, *J. Am. Chem. Soc.*, 2006, **128**, 8728–8729; (*e*) G. Yin, A. M. Danby, D. Kitko, J. D. Carter, W. M. Scheper and D. H. Busch, *J. Am. Chem. Soc.*, 2007, **129**, 1512–1513.
4 (*a*) T. H. Parsell, M.-Y. Yang and A. S. Borovik, *J. Am. Chem. Soc.*, 2009, **131**, 2762–2763; (*b*) Y. Wang, S. Shi, H. Wang, D. Zhu and G. Yin, *Chem. Commun.*, 2012, **48**, 7832–7834; (*c*) S. Shi, Y. Wang, A. Xu, H. Wang, Z. Dajian, S. B. Roy, T. A. Jackson, D. H. Busch and G. Yin, *Angew. Chem., Int. Ed.*, 2011, **50**, 7321–7324.
5 (*a*) K. Ayougou, E. Bill, J. M. Charnock, C. D. Garner, D. Mandon, A. X. Trautwein, R. Weiss and H. Winkler, *Angew. Chem., Int. Ed. Engl.*, 1995, **34**, 343–346; (*b*) T. Kurahashi, A. Kikuchi, T. Tosha, Y. Shiro, T. Kitagawa and H. Fujii, *Inorg. Chem.*, 2008, **47**, 1674–1686; (*c*) T. Kurahashi, A. Kikuchi, Y. Shiro, M. Hada and H. Fujii, *Inorg. Chem.*, 2010, **49**, 6664–6672.
6 C. M. Hansel, C. A. Zeiner, C. M. Santelli and S. M. Webb, *Proc. Natl. Acad. Sci. U. S. A.*, 2012, **109**, 12621–12625.
7 S. Chattopadhyay, R. A. Geiger, G. Yin, D. H. Busch and T. A. Jackson, *Inorg. Chem.*, 2010, **49**, 7530–7535.
8 T. M. Rajendiran, J. W. Kampf and V. L. Pecoraro, *Inorg. Chim. Acta*, 2002, **339**, 497–502.
9 G. Yin, A. M. Danby, D. Kitko, J. D. Carter, W. M. Scheper and D. H. Busch, *J. Am. Chem. Soc.*, 2008, **130**, 16245–16253.
10 E. J. Klinker, S. Shaik, H. Hirao and L. Que, *Angew. Chem., Int. Ed.*, 2009, **48**, 1291–1295.
11 A potential complication for this rate comparison is the difference in solvents (Table S8; ESI†). **2** reacts with DHA at essentially the same rate in 1 : 1 $CF_3CH_2OH$ : $CH_2Cl_2$ (ESI†), though the KIE drops to 8.7. In other solvents **2** has limited stability or does not form.
12 (*a*) K.-B. Cho, S. Shaik and W. Nam, *J. Phys. Chem. Lett.*, 2012, **3**, 2851–2856; (*b*) J. Chen, Y.-M. Lee, K. M. Davis, X. Wu, M. S. Seo, K.-B. Cho, H. Yoon, Y. J. Park, S. Fukuzumi, Y. N. Pushkar and W. Nam, *J. Am. Chem. Soc.*, 2013, DOI: 10.1021/ja312113p.
13 In the absence of any substrate, the thermal decay of **2** yields a similar product, as judged by electronic absorption spectroscopy.
14 J. M. Mayer, *Acc. Chem. Res.*, 2010, **44**, 36–46.

 